scientific reports

Check for updates

OPEN

Enhanced organic matter removal and fouling mitigation in seawater desalination using electrocoagulation pretreatment using ZnO coated Fe electrodes

Saeid. Nickabadi[1]✉, Behrang Golmohammadi[2]✉ & Mohammadreza Hadavi[1]

This study introduces a novel application of electrocoagulation (EC) as a pretreatment method for seawater desalination, uniquely focusing on reducing organic and biological fouling in reverse osmosis membranes. The EC process was investigated as an alternative to conventional approaches such as chemical coagulation, chlorination, and fouling inhibitors. EC was conducted in a batch cell using iron electrodes. The effectiveness of the EC process in removing organic matter from water was monitored by measuring absorbance UV254 and dissolved organic carbon (DOC), as well as total hardness. Various operational parameters, including mixing speed, current density, initial pH, and electrode spacing, were examined. Results demonstrated that increasing current density and decreasing pH enhanced the removal of organic matter from seawater via EC. The process achieved a 62% reduction in DOC and a 59.7% reduction in absorbance, indicating that higher current density is more favorable for these reactions. However, the reduction in total hardness was relatively low at approximately 11.2%, suggesting that EC is not suitable for reducing water hardness. Overall, the experimental findings highlight the high potential of electrocoagulation as a pretreatment method for mitigating organic and biological fouling of reverse osmosis membranes due to its effectiveness in removing dissolved organic matter and microorganisms from seawater.

Keywords Electrocoagulation, Seawater, Desalination, Dissolved organic carbon

Seawater preprocessing with electrocoagulation is a technique used to remove suspended solids, heavy metals, and other contaminants from seawater before further desalination or treatment processes[1]. The process begins with the application of an electrical current to the seawater, which causes the dissolved ions and suspended particles to coagulate and form larger, easily removable flocs[2–4]. This is achieved through the use of a sacrificial anode, typically made of aluminum or iron, which dissolves and releases metal ions into the water[5]. These metal ions then react with the contaminants, causing them to destabilize and aggregate[6]. The coagulated particles, or flocs, formed during the electrocoagulation process then undergo flocculation, where they are agglomerated into larger, more easily settleable particles[7]. This can be achieved by the addition of flocculants, such as polymers, which help bridge the smaller flocs together. The larger flocs settle out of the water due to gravity, leaving a clarified supernatant that can be further processed, such as through membrane filtration or thermal desalination[8].

The key advantages of using electrocoagulation for seawater preprocessing include the effective removal of suspended solids, heavy metals, and other contaminants, the lack of a need for the addition of chemicals, as the process relies on the electrochemical generation of coagulants, and the compact and relatively simple system design[9]. Additionally, there is the potential for energy recovery from the electrochemical process. Electrocoagulation is often used as a pretreatment step in seawater desalination plants to improve the performance and efficiency of the downstream processes, such as reverse osmosis or multi-stage flash distillation[10]. The specific design and operating parameters of an electrocoagulation system for seawater preprocessing will depend on the water quality, desired removal efficiency, and the overall system requirements, and it's important to conduct

[1]Faculty of Mechanical Engineering, University of Imam Khomeini Marine Sciences, Nowshahr, Iran. [2]Department of Physical Chemistry, Faculty Chemistry, University of Tabriz, Tabriz, Iran. ✉email: s.nikabadi@ikhnsu.ac.ir; behrangrose@gmail.com; b.golmohammadi@tabrizu.ac.ir

thorough testing and optimization to ensure the system meets the necessary performance and cost-effectiveness criteria[11].

The application of ZnO (zinc oxide) coated on stainless steel electrodes has emerged as a promising approach for enhancing the performance and efficiency of seawater electrocoagulation[12,13]. One of the primary advantages of ZnO is its ability to improve the coagulation and flocculation processes during the electrocoagulation of seawater[14]. The ZnO coating acts as a catalyst, accelerating the dissolution of the sacrificial anode material (typically aluminum or iron) and the subsequent formation of metal hydroxides[15]. These metal hydroxides effectively capture and remove suspended solids, heavy metals, and other contaminants from the seawater[16]. Additionally, the ZnO coating can improve the corrosion resistance of the stainless steel electrodes, increasing their lifespan and reducing the need for frequent replacement[17]. This can contribute to the overall cost-effectiveness and operational longevity of the electrocoagulation system. The enhanced charge transfer between the electrodes and the seawater, facilitated by the ZnO coating, can also lead to more efficient electrochemical reactions and better coagulation performance[18].

In comparison to other nanomaterials, such as titanium dioxide (TiO2), graphene and graphene oxide, iron oxide (Fe3O4), and cerium oxide (CeO2), ZnO exhibits several advantages[19]. Firstly, while materials like TiO2 and CeO2 have strong catalytic properties, ZnO has been shown to have excellent catalytic activity and can effectively enhance the coagulation and flocculation processes during electrocoagulation[20]. Secondly, the ZnO coating can improve the charge transfer between the electrodes and the seawater, resulting in more efficient electrochemical reactions compared to some other nanomaterials[21]. Additionally, ZnO can be effective in the removal of a wide range of contaminants, including suspended solids, heavy metals, and even certain organic compounds and microorganisms, making it a versatile choice for seawater treatment[22]. Finally, ZnO is generally a more cost-effective material compared to some of the other nanomaterials, which can be an important consideration for large-scale seawater electrocoagulation applications[23]. While the other nanomaterials offer unique advantages, such as the strong photocatalytic properties of TiO_2 or the excellent adsorption capabilities of graphene-based materials, the overall performance and cost-effectiveness of ZnO-coated electrodes make it a highly attractive option for seawater electrocoagulation. The use of composite nanomaterials, combining the benefits of multiple nanomaterials, may also be a viable approach to further optimize the treatment efficiency and meet specific water quality requirements.

Despite advancements in electrocoagulation with ZnO-coated electrodes, its application as a pretreatment method for seawater desalination to reduce organic and biological fouling in reverse osmosis membranes remains underexplored. This study addresses this gap by systematically evaluating multiple operational parameters (mixing speed, current density, initial pH, and electrode spacing) and their combined effect on the removal of dissolved organic carbon (DOC) and UV254 absorbance. For the first time, we demonstrate a quantitative relationship between current density, pH, and the removal efficiency of organic matter in seawater for reducing membrane fouling. This approach is critical for optimizing pretreatment processes in seawater reverse osmosis systems. Furthermore, our findings on the limited effectiveness of EC in reducing water hardness provide new insights into the application scope of EC, which has practical implications for desalination pretreatment design.

The environmental and operational challenges of traditional pretreatment methods, such as chemical coagulation and chlorination, are discussed to justify the need for alternative methods like EC. The potential advantages of ZnO-coated electrodes in EC are elaborated, including their role in enhancing removal efficiency and reducing fouling. By addressing these gaps, this study contributes to advancing the understanding and application of ZnO-coated electrodes for seawater electrocoagulation.

Materials and methods

Saline water samples

The properties of the seawater used in this research are detailed in Table 1 (simulated with the properties of Persian Gulf water at a depth between 1 and 2 m from the water surface).

Dissolved organic carbon (DOC) was measured using a total organic carbon (TOC) analyzer (Model 820, Sievers Instruments, USA). Samples were filtered through 0.45 µm pore size filters prior to analysis to remove particulate matter. Calibration was performed using standard solutions of known organic carbon concentrations, and the results are reported as the average of triplicate measurements to ensure accuracy.

Physicochemical Parameters	Values
Conductivity	52.4 mS/cm
Salinity	2500 mg/L
TDS	35,200 mg/L
DOC	1.34 mg/L
Total Hardness	2300 mg/L
UV 254	1.95 m^{-1}
pH	8

Table 1. Features of saline water.

Setup of experiment

The experimental setup for the electrocoagulation (EC) method used in this study is illustrated in Fig. 1. The experiment was conducted using a reactor with dimensions of 15 cm in width, 15 cm in length, and 10 cm in depth. Six iron plates, wired in parallel with the main power supply, were used as electrodes in a monopolar configuration for both the anodes and cathodes. Each electrode plate had dimensions of 10 cm by 5 cm, with a thickness of 0.1 cm, providing a surface area of 50 cm^2 per electrode. The electrodes were submerged in saltwater for the treatment process. The anode and cathode groups were connected to the negative and positive terminals

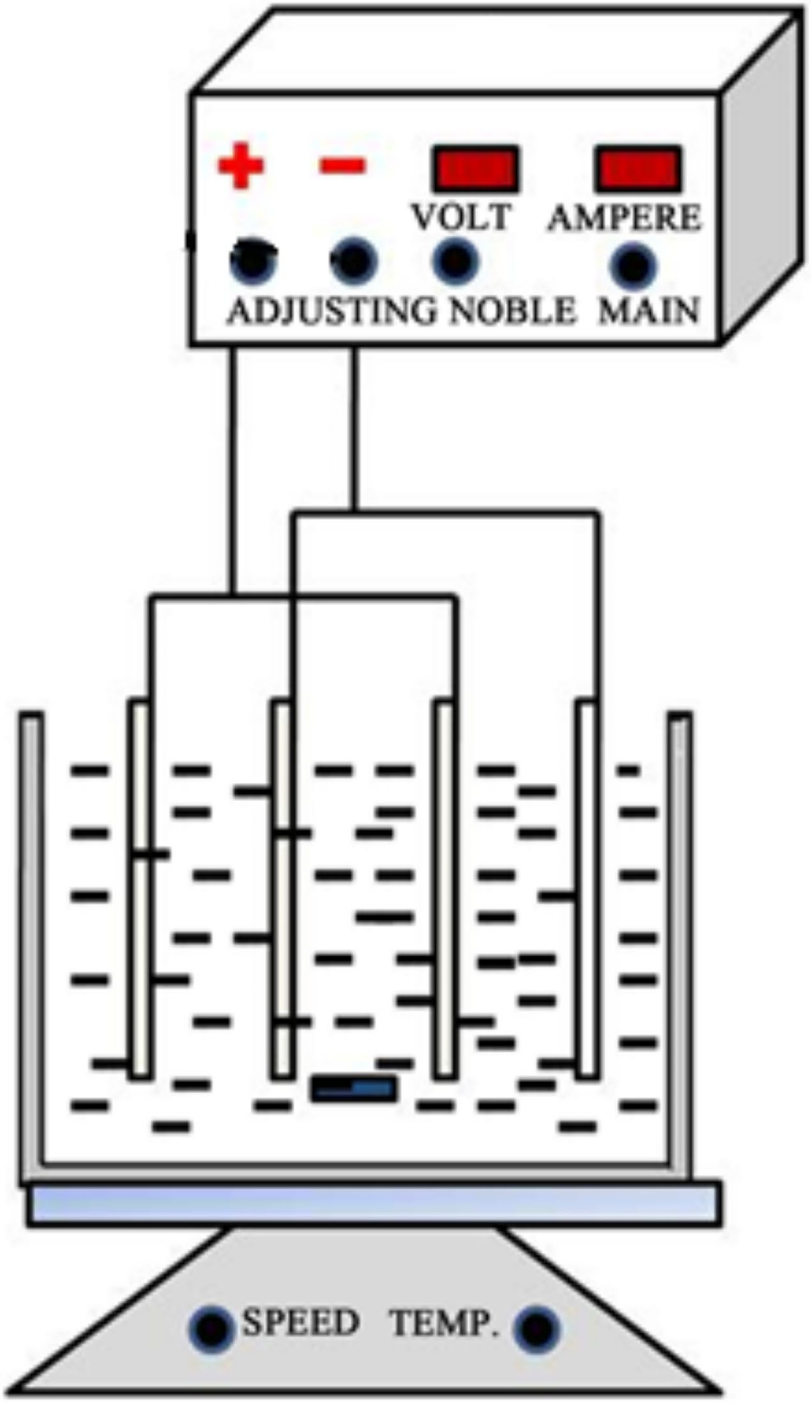

Fig. 1. Experimental setup of the electrocoagulation (EC) process.

of a DC power supply, respectively. The stirring speed during the experiments was controlled using a magnetic stirrer to ensure uniform mixing and proper contact between the electrodes and the seawater. Each experiment was conducted at least three times.

Substrate preparation

Prior to deposition, the substrates underwent a mechanical polishing process using abrasive papers with progressively finer grits of 600, 800, 1000, 1200, 2000, and 2400. Following polishing, the substrates were ultrasonically cleaned using acetone and deionized water, each for 10 min at 60 °C. The cleaned substrates were then dried at 100 °C for 1 h before proceeding to the deposition process.

Preparation of stainless-steel surface

The ZnO solution was prepared using zinc acetate dihydrate ($Zn(CH_3COO)_2{\cdot}2\,H_2O$) (Fluka, > 99.0%), ethanol, and monoethanolamine (C_2H_7NO, MEA). The concentration of Zn^{2+} in the solutions was set to 0.4 M. The solutions were stirred continuously for 1 h and then aged for 24 h. ZnO nanoparticle coatings were applied using the dip-coating method. Substrates were immersed in the ZnO solution and withdrawn at a speed of 1 $mm{\cdot}s^{-1}$. The coated substrates were then heated at 400 °C for 10 min. This process of dip coating and drying was repeated four times to achieve the desired thickness. Finally, the obtained thin films were calcined at 450 °C for 1 h. In this study, a layer-by-layer (LbL) approach was used to deposit four films[24].

Characterizations

X-ray diffraction (XRD) patterns were measured on a PANalytical X-ray diffractometer using Cu Kα radiation (λ = 1.5406 Å). Scanning electron microscope (SEM) images were collected by a field-emission SEM (FE-SEM, MIRA3-XMU, TESCAN). Fourier transform infrared (FT-IR) spectra of the materials were obtained with an ABB BOMER MB series spectrophotometer. The study involves assessing saltwater contaminants both before and during treatment using specific processes and instruments. To determine the acidity or alkalinity of the saltwater, a pH meter (model pHM84) is used. The concentration of dissolved substances is measured with a TDS meter (model TDS-EZ, HM Digital). Electrical conductivity, which indicates the level of ionized substances in the water, is assessed using the HANNA HI-99,301 instrument. Additionally, the concentration of chloride ions is quantified through titration using Mohr's Method. These methods collectively ensure a comprehensive analysis of water quality by evaluating key parameters affecting saltwater treatment.

Results and discussion

Physical characterizations

The successful coating of ZnO on the surface of SS316 stainless steel was confirmed through Scanning Electron Microscopy (SEM) analysis (Fig. 2a and b). SEM images revealed a uniform and well-adhered ZnO layer, characterized by a continuous and homogeneous distribution of nanoparticles across the substrate surface. The micrographs showed that the ZnO nanoparticles exhibited a distinct morphology, typically indicative of the crystalline nature of the coating[25]. The high-resolution SEM images highlighted the fine details of the ZnO nanostructures, confirming their successful deposition and the absence of significant defects or discontinuities

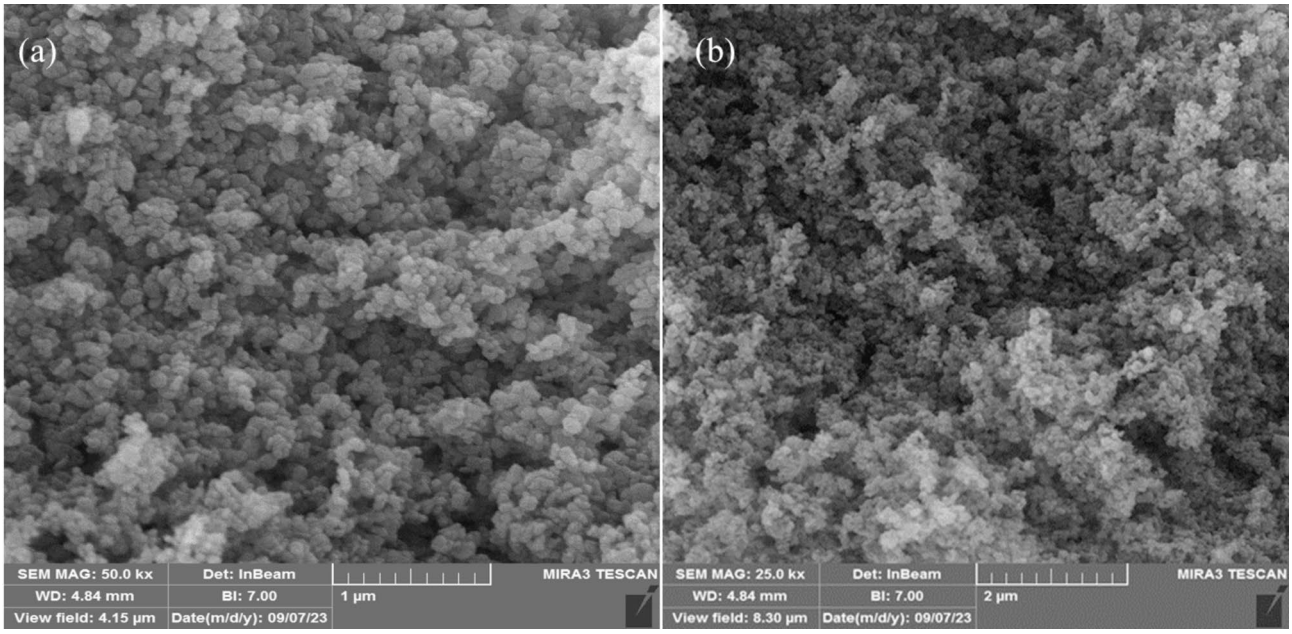

Fig. 2. SEM images of coating of ZnO on the surface of SS316 at different scales.

in the coating. This uniform coverage and the nanoscale features observed under SEM underscore the efficacy of the dip-coating process employed in this study for synthesizing ZnO coatings on SS316 substrates.

The successful coating of ZnO on the surface of SS316 stainless steel, as confirmed by Scanning Electron Microscopy (SEM) analysis, can be attributed to the efficacy of the dip-coating process employed in the study. The SEM images revealed a uniform and well-adhered ZnO layer with a continuous and homogeneous distribution of nanoparticles across the substrate surface, exhibiting a distinct morphology indicative of the crystalline nature of the coating[26]. The high-resolution SEM images further highlighted the fine details of the ZnO nanostructures, confirming their successful deposition and the absence of significant defects or discontinuities in the coating, underscoring the suitability of the dip-coating technique for synthesizing ZnO coatings on SS316 substrates. The findings of this study are in agreement with previous reports in the literature[27]. As shown in Fig. 3, the FT-IR spectrum of the ZnO coating on 316 SS alloy reveals several characteristic absorption bands. Specifically, the band at 440 cm^{-1} is indicative of the ZnO stretching vibration, while the band at 3465 cm^{-1} corresponds to the O-H stretching vibration. Furthermore, a weak band at 1512 cm^{-1} is attributed to the H-O-H bending vibration. The presence of these bands collectively confirms the successful synthesis of ZnO nanoparticles on the steel substrate.

The specific FT-IR spectrum results observed for the ZnO coating on the 316 SS alloy. The band at 440 cm^{-1} is indicative of the characteristic stretching vibration of the Zn-O bond, indicating the presence of the ZnO phase on the surface. Furthermore, the band at 3465 cm^{-1} corresponds to the stretching vibration of the hydroxyl (O-H) groups, suggesting the incorporation of hydroxyl groups within the ZnO coating, likely due to the adsorption of water molecules or the presence of surface hydroxyl groups. Additionally, a weak band at 1512 cm^{-1} is attributed to the bending vibration of the H-O-H groups, further confirming the presence of water-related species within the ZnO coating, which can be associated with the hydroxyl groups identified in the O-H

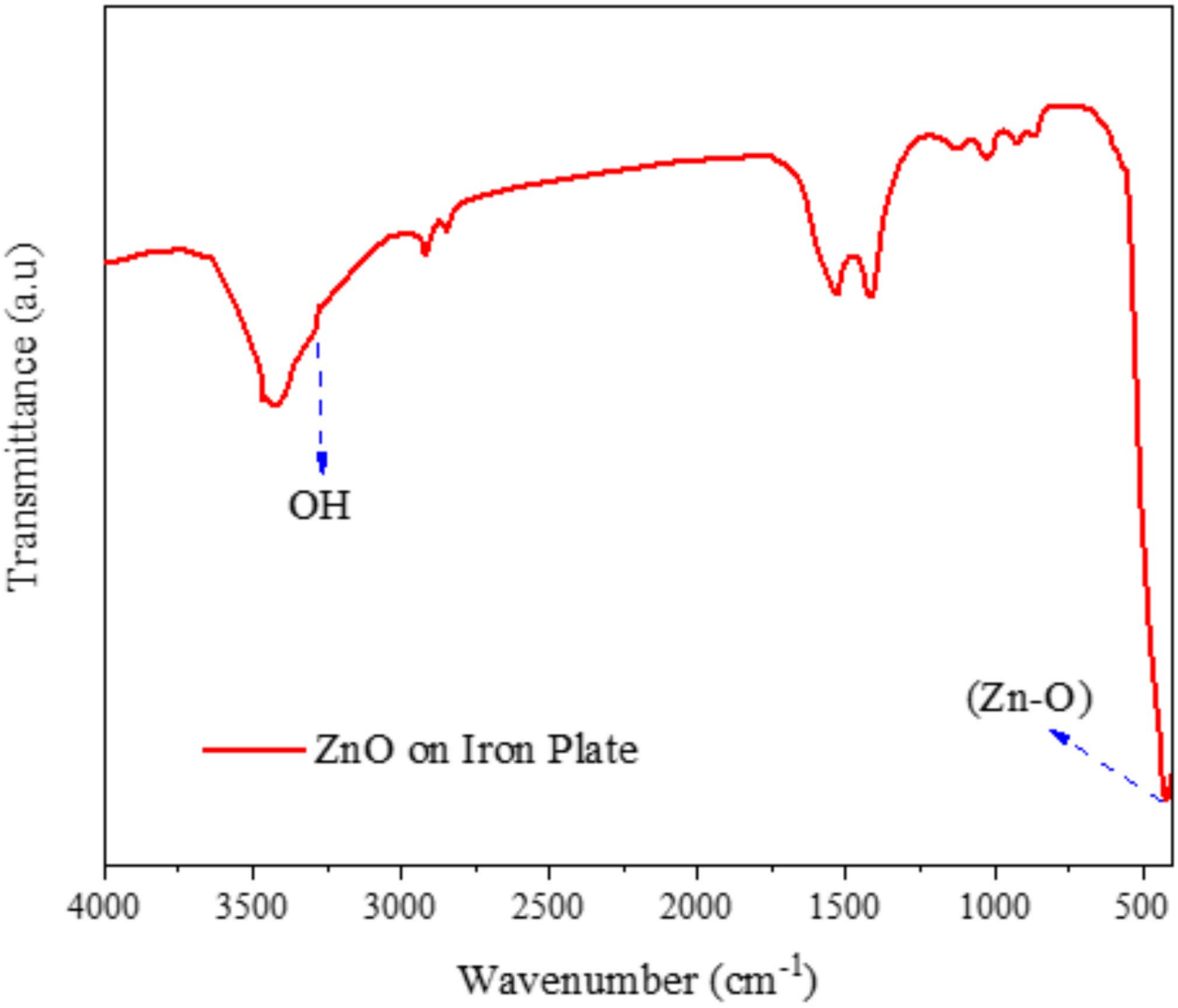

Fig. 3. FT-IR spectra of the ZnO coating on 316 SS alloy.

stretching vibration. The collective presence of these characteristic FT-IR bands provides strong evidence for the successful synthesis of ZnO nanoparticles on the 316 SS alloy substrate.

The FT-IR spectra of ZnO nanoparticles have been extensively characterized in prior studies, revealing various absorption peaks indicative of functional groups and chemical bonds. One study reported absorption peaks at 3438, 2918, 2367, 1634, 1446, 1033, 876, and 701 cm^{-1}. Among these, the peak at 1033 cm^{-1} is characteristic of Zn-O bonding, while peaks at 1634 and 1446 cm^{-1} correspond to the stretching vibrations of C = C bonds in the capping agent. The presence of C-O stretching was identified at 2367 cm^{-1}, and peaks at 3438 cm^{-1} were attributed to O-H stretching vibrations. These findings confirm the presence of Zn-O and other associated groups within the nanoparticles[28].

In another study, the FT-IR spectra of pure ZnO and Cr-doped ZnO nanoparticles showed a broad absorption peak around 3450 cm^{-1}, attributed to O-H stretching vibrations, and a peak at 1643 cm^{-1}, corresponding to H-O-H bending vibrations from adsorbed water molecules. The Zn-O stretching vibration was observed at 483 cm^{-1}, while the Cr-O stretching vibration appeared at 880 cm^{-1}, confirming the incorporation of Cr atoms into the ZnO lattice. The shifts in absorption peaks due to Cr doping were consistent with previously reported values, further validating the structural changes in ZnO nanoparticles upon doping[29].

A separate investigation of synthesized ZnO nanoparticles identified absorption peaks at 3437.8, 2925.8, 1595.8, 1383.7, 1355.5, 1118.1, 1005.3, 863.3, 776.8, 700.6, and 575.9 cm^{-1}. The peak at 575.9 cm^{-1} corresponded to Zn-O stretching vibrations, while the peak at 1005.3 cm^{-1} was attributed to the stretching vibration of either C-N bonds in primary amines or C-O bonds in primary alcohols. Peaks at 1118.1, 1355.5, and 1383.7 cm^{-1} were linked to primary and secondary alcohols, while the peak at 1595.8 cm^{-1} was associated with aromatic nitro compounds and alkyl vibrations. Peaks at 2925.8 and 3437.8 cm^{-1} were ascribed to hydroxyl stretching vibrations, further confirming the presence of hydroxyl groups within the nanoparticles[30].

In the present study, the FT-IR spectrum of the ZnO coating on 316 SS alloy revealed characteristic absorption bands that confirmed the successful synthesis of ZnO nanoparticles on the substrate. The band at 440 cm^{-1} was attributed to Zn-O stretching vibrations, while the broad band at 3465 cm^{-1} corresponded to O-H stretching vibrations, suggesting the incorporation of hydroxyl groups likely due to water adsorption or surface hydroxyl groups. Additionally, a weak band at 1512 cm^{-1} was identified as H-O-H bending vibrations, further supporting the presence of water-related species within the ZnO coating. These observations align with previous studies and provide strong evidence for the successful formation of ZnO on the alloy surface.

To compare and verify the synthesis of zinc nanoparticles on the iron sheet, two X-ray diffraction (XRD) analyses were conducted: one on the bare iron sheet and another on the iron sheet loaded with zinc nanoparticles. The results of these analyses correspond well with those reported in the literature, confirming the successful loading of zinc nanoparticles on the iron sheet. Figure 4.a displays the XRD analysis of the bare iron sheet. The peaks at 44.67°, 52.24°, and 78.31° correspond to the (111), (200), and (220) crystal planes, indicating the presence of austenite. Additionally, the peaks at 47.25° and 73.35° correspond to the (110) and (200) crystal planes, indicating the presence of ferrite. Figure 4.b presents the XRD pattern of the ZnO nanostructure deposited on the 316 stainless steel (316 SS) sheet. This pattern matches well with the JCPDS reference pattern (1451-036-00), indicating a hexagonal wurtzite structure with a P63mc space group. The sharp XRD peaks suggest that ZnO is highly crystalline. The peaks observed at 31.73°, 34.65°, 36.24°, 47.58°, 56.57°, 62.81°, 66.18°, 67.98°, and 69.11° correspond to the (100), (002), (101), (102), (110), (103), (200), (112), and (201) crystal planes, respectively. Therefore, the changes in the XRD pattern, along with comparisons to the literature, indicate the successful synthesis of zinc nanoparticles on the 316 SS sheet.

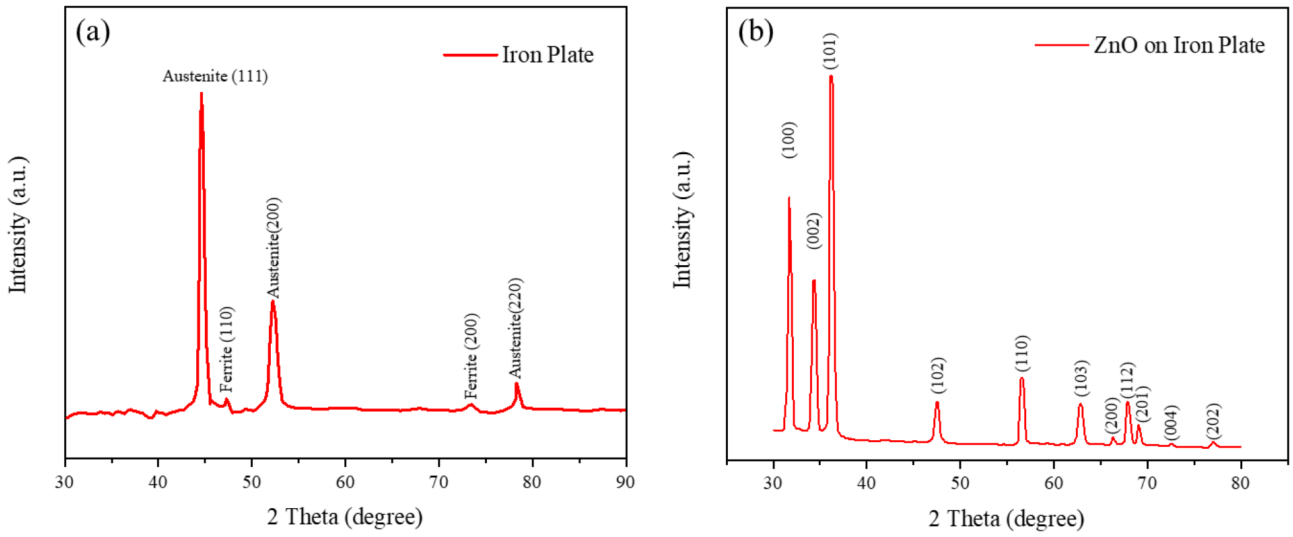

Fig. 4. XRD patterns of (**a**) the bare 316 stainless steel (316 SS) and (**b**) ZnO nanostructure deposited on the 316 stainless steel (316 SS).

The changes observed in the XRD pattern between the bare iron sheet and the iron sheet loaded with zinc nanoparticles, along with the comparison to the literature references, provide strong evidence for the successful synthesis of zinc nanoparticles on the 316 SS substrate. The highly crystalline nature of the ZnO nanoparticles, as indicated by the sharp XRD peaks, further supports the efficacy of the synthesis process employed in the study.

Parameters analysis

The efficiency of the electrocoagulation (EC) process was evaluated based on various operational parameters. Key parameters selected for assessment included the reduction of dissolved organic carbon (DOC) and the reduction of UV254 absorbance, both as functions of EC operating conditions such as current density, pH, electrode spacing (d), and mixing rate[31]. The removal efficiency for each parameter was calculated using the following formula:

$$DOC\ Removal\ (\%) = \frac{DOC\ (t=0) - DOC\ (t)}{DOC\ (t=0)} \times 100 \tag{1}$$

$$UV_{254}\ Removal\ (\%) = \frac{UV_{254}\ (t=0) - UV_{254}\ (t)}{UV_{254}\ (t=0)} \times 100 \tag{2}$$

Effect of mixing on electrocoagulation system

Mixing conditions significantly influence the efficiency of electrocoagulation in pollutant reduction, especially when the maximum capacity for adsorption, co-precipitation, or neutralization of iron hydroxides is not achieved due to poor mass transfer[32]. This study evaluated the effect of mechanical mixing on the removal of organic matter from seawater by applying mixing speeds of 45, 90, and 180 rpm at a current density of 12 mA/cm^2 and a pH of 8. As shown in Fig. 5, increasing the mixing speed from 45 to 90 rpm slightly enhanced the DOC removal efficiency from 48.0 to 49.0% at 40 min and from 54.0 to 55.6% at 80 min of treatment time. Further increasing the mixing speed from 90 to 180 rpm resulted in only a marginal change in DOC removal efficiency. Notably, no significant change in DOC removal efficiency was observed after 20 min of treatment. The most significant differences in the removal efficiencies were observed within the first 100 min, where both 90 rpm and 180 rpm exhibited similar performance, indicating that 90 rpm is the optimized mixing speed. Although the differences

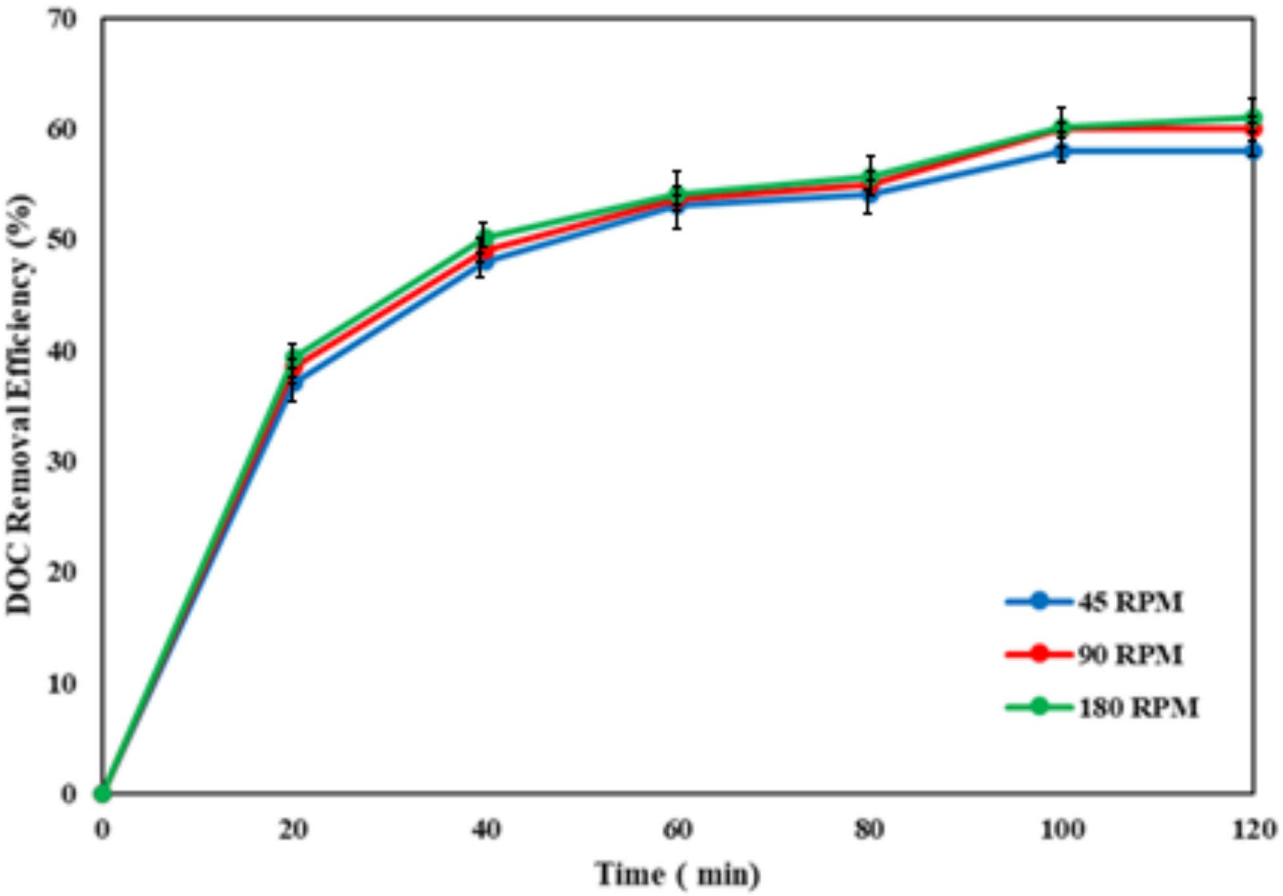

Fig. 5. Effect of mixing rate on DOC removal with operating conditions: initial pH = 8, current density = 12 mA cm^{-2}, electrode distance = 4 cm.

between the curves were minor, the objective was to minimize purification time to reduce both Fe^{2+} release and power consumption. A mixing speed of 90 rpm improved the dispersion of iron hydroxide species throughout the entire electrocoagulation cell compared to 45 rpm, ensuring a more uniform treatment process.

The improved performance at 90 rpm can be attributed to the better dispersion of iron hydroxide species throughout the entire electrocoagulation cell compared to the 45 rpm mixing speed. The more uniform distribution of the iron hydroxide species ensures a more effective treatment process, leading to enhanced DOC removal[33]. Overall, the study's findings demonstrate the importance of optimizing the mixing conditions in the electrocoagulation process to achieve the desired removal of organic matter from seawater, while also considering the practical aspects of the system's operation.

Effect of current density on electrocoagulation process

The efficiency of dissolved organic carbon (DOC) removal from seawater by the electrocoagulation process increased significantly with higher applied current densities. As illustrated in Fig. 6, the DOC removal rates were measured at 21%, 37%, 39%, 43%, 47%, and 57% for current densities of 2, 4, 8, 12, 16, and 20 mA/cm^2, respectively, over a treatment time of 60 min. These results indicate a clear positive correlation between current density and DOC removal efficiency, with higher current densities enhancing the electrocoagulation process's effectiveness. The increased electrical input likely promotes greater production of coagulant species and improves the destabilization of dissolved organic compounds, leading to more effective removal from the seawater.

The study's findings on the impact of current density on the efficiency of dissolved organic carbon (DOC) removal from seawater by the electrocoagulation process are quite interesting and insightful. As shown in Fig. 6, the DOC removal rates were measured at different current densities over a treatment time of 60 min. The results clearly demonstrate a positive correlation between the applied current density and the DOC removal efficiency: at a current density of 2 mA/cm^2, the DOC removal rate was 21%. Increasing the current density to 4 mA/cm^2 resulted in a DOC removal rate of 37%. Further increasing the current density to 8 mA/cm^2 led to a DOC removal

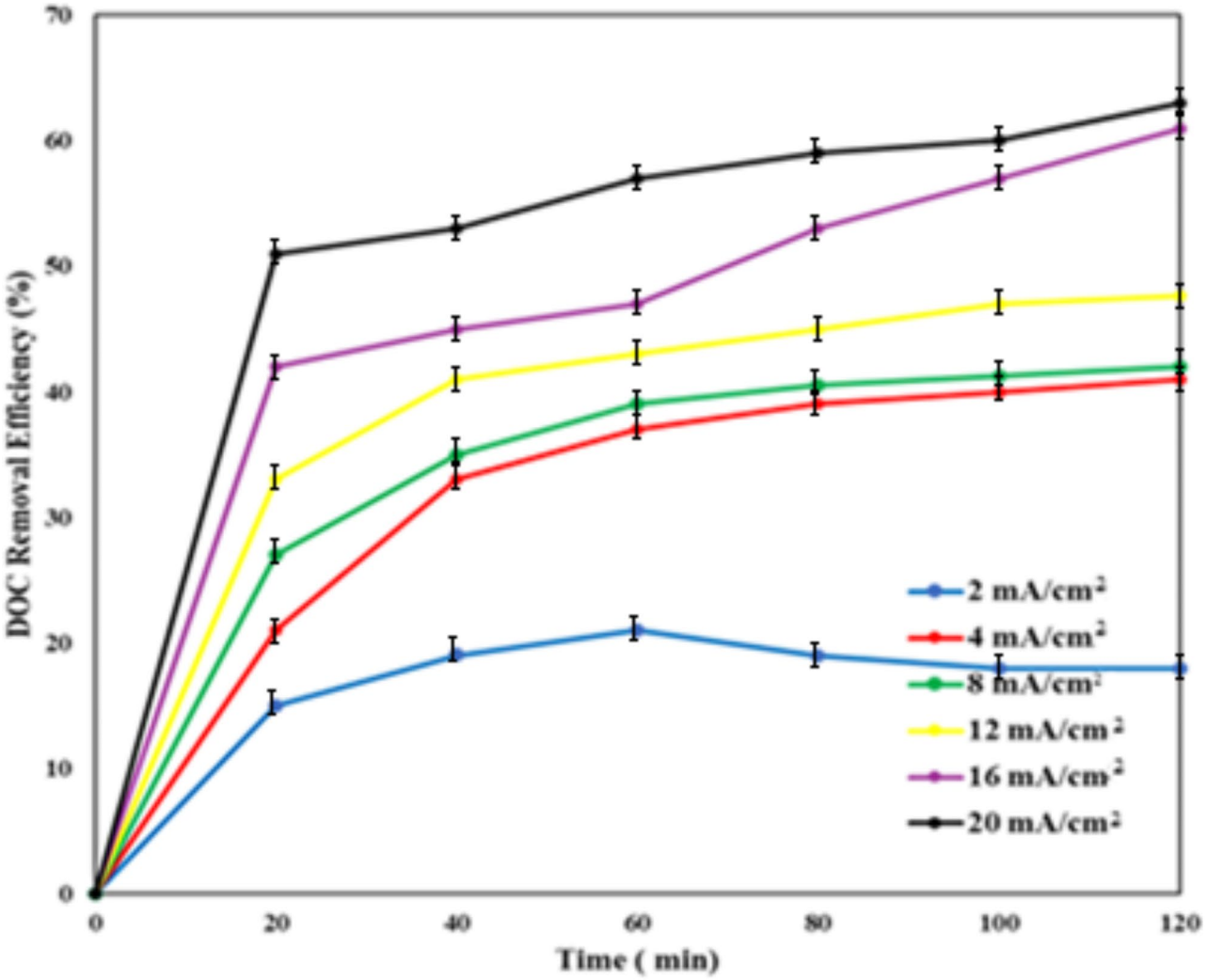

Fig. 6. Effect of current density on DOC removal with operating conditions: initial pH = 8, mixing speed = 90 rpm, electrode distance = 4 cm.

rate of 39%. At a current density of 12 mA/cm^2, the DOC removal rate increased to 43%. Applying a current density of 16 mA/cm^2 improved the DOC removal to 47%. The highest current density tested, 20 mA/cm^2, achieved the highest DOC removal rate of 57%. These results clearly indicate that as the current density applied to the electrocoagulation process increases, the efficiency of DOC removal from seawater also significantly improves[34]. The underlying mechanism behind this observation is that higher current densities promote the enhanced production of coagulant species, such as iron hydroxides, within the electrocoagulation system[35]. These coagulant species play a crucial role in the destabilization and removal of dissolved organic compounds from the seawater[36]. When a higher current density is applied, it leads to an increased rate of electrochemical reactions at the electrode-electrolyte interface[37]. This, in turn, results in a greater amount of iron ions (Fe^{2+} or Fe^{3+}) being released into the solution from the sacrificial anode. These iron ions then undergo hydrolysis, forming various iron hydroxide species (e.g., $Fe(OH)_3$, $Fe(OH)_2$) that act as effective coagulants[38]. The increased generation of these coagulant species improves the destabilization and aggregation of the dissolved organic compounds present in the seawater[39]. The larger, denser flocs formed by this process are then more easily removed from the solution, leading to the enhanced DOC removal observed at higher current densities[40,41]. Furthermore, the increased electrical input at higher current densities may also contribute to the improved performance by enhancing other electrochemical processes, such as electrochemical oxidation, that can help break down and remove the organic matter.

The reduction of UV254 absorbance from seawater, indicating the partial removal of aromatic organic matter such as humic and fulvic acids, exhibited a similar trend to DOC removal over time, as shown in Fig. 5. The UV254 reduction improved with increasing current density, with reductions of 32%, 35%, 37%, 40%, 43%, and 47% observed for current densities of 2, 4, 8, 12, 16, and 20 mA/cm^2, respectively, over 60 min. Figure 7 indicates that current load, defined as the product of current and time, is not a suitable parameter for scaling purposes, as all curves tend to plateau at values dependent on current density. This suggests that the roles of electrolysis time and current are not equivalent in the electrocoagulation process[42]. The removal of contaminants appears to be more sensitive to the cell potential, which depends on current density rather than treatment time[43]. This

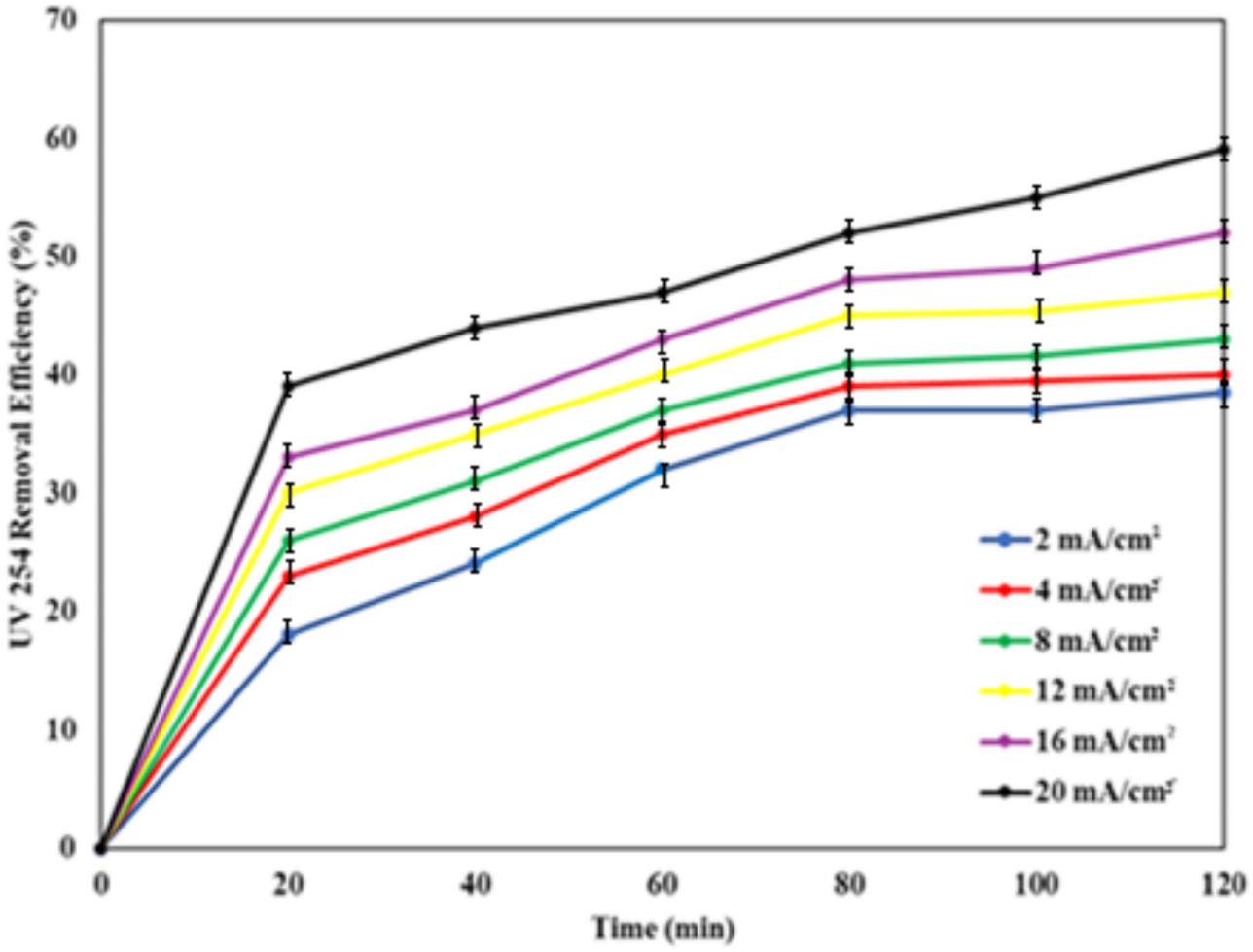

Fig. 7. Effect of current density on UV254 removal with operating conditions: initial pH = 8, mixing speed = 90 rpm, electrode distance = 4 cm.

highlights the importance of optimizing current density to enhance the efficiency of aromatic organic matter removal during electrocoagulation.

The removal of organic matter from seawater through electrocoagulation is likely facilitated by three primary mechanisms: adsorption, charge neutralization, and electro-oxidation[44]. Higher current densities generate significant quantities of metal hydroxide species, which effectively adsorb organic matter and neutralize the organic load in seawater[45]. Additionally, elevated current densities promote substantial oxidation of organic compounds. The study's findings regarding the reduction of UV254 absorbance, which is an indicator of the partial removal of aromatic organic matter such as humic and fulvic acids, provide additional insights into the electrocoagulation process[46]. As shown in Fig. 5, the UV254 reduction exhibited a similar trend to the DOC removal over time, with the efficiency improving as the current density increased. Specifically, at a current density of 2 mA/cm^2, the UV254 reduction was 32%. Increasing the current density to 4 mA/cm^2 resulted in a UV254 reduction of 35%. Further increasing the current density to 8 mA/cm^2 led to a UV254 reduction of 37%. At a current density of 12 mA/cm^2, the UV254 reduction increased to 40%. Applying a current density of 16 mA/cm^2 improved the UV254 reduction to 43%. The highest current density tested, 20 mA/cm^2, achieved the highest UV254 reduction of 47%. These findings indicate that the removal of aromatic organic matter, as measured by the UV254 absorbance reduction, follows a similar pattern to the overall DOC removal observed earlier. Higher current densities enhance the electrocoagulation process's effectiveness in removing these types of organic compounds from the seawater.

It has also observed an interesting phenomenon related to the scaling of the electrocoagulation process, as illustrated in Fig. 7. The graph shows that current load, defined as the product of current and time, is not a suitable parameter for scaling purposes, as all the curves tend to plateau at values dependent on the current density. This suggests that the roles of electrolysis time and current are not equivalent in the electrocoagulation process. The removal of contaminants, including aromatic organic matter, appears to be more sensitive to the cell potential, which depends on the current density rather than the treatment time[47]. This finding highlights the importance of optimizing the current density to enhance the efficiency of aromatic organic matter removal during the electrocoagulation process. Simply increasing the treatment time may not necessarily lead to a proportional increase in the removal efficiency, as the process is more dependent on the applied current density.

In summary, the study's results demonstrate that the reduction of UV254 absorbance, which is indicative of the partial removal of aromatic organic matter, follows a similar trend to the overall DOC removal, with higher current densities leading to more effective removal. Additionally, the researchers found that current load is not a suitable parameter for scaling the electrocoagulation process, as the removal efficiency is more sensitive to the current density than the treatment time[48]. This emphasizes the importance of optimizing the current density to maximize the efficiency of aromatic organic matter removal during electrocoagulation. Consequently, the highest removal efficiencies for dissolved organic carbon (DOC) and UV254 absorbance were observed at the highest current density. After 80 min of treatment, both DOC and UV254 removal efficiencies showed minimal changes with further increases in treatment time. Specifically, a current density of 20 mA/cm^2 achieved a DOC removal efficiency of 63%, while UV254 absorbance was reduced by 59%. These results underscore the critical role of current density in optimizing the effectiveness of electrocoagulation for organic matter removal in seawater.

The final physicochemical parameters were measured as a function of current density, as shown in Table 2. Electrical conductivity and salinity remained almost constant, with only a slight decrease observed as the applied current density increased; however, these changes were not statistically significant. The reduction in salinity can be attributed to the adsorption of anions and cations onto iron hydroxides and the precipitation of salts such as $CaCO_3$, $CaSO_4$, $MgCO_3$, and $MgSO_4$[49]. This adsorption and precipitation process leads to a decrease in electrical conductivity. Despite the decrease in pH and the corresponding increase in H^+ concentration, the overall effect on electrical conductivity is minimal because the salinity and hardness of seawater are so high that their reduction cannot be fully offset by the decrease in pH. This suggests that the primary mechanisms for reducing salinity and conductivity involve the removal of dissolved salts through electrocoagulation.

Consequently, the study found that the highest removal efficiencies for dissolved organic carbon (DOC) and UV254 absorbance were observed at the highest current density tested. After 80 min of treatment, both DOC and UV254 removal efficiencies showed minimal changes with further increases in treatment time. Specifically, a current density of 20 mA/cm^2 achieved a DOC removal efficiency of 63%, while UV254 absorbance was reduced by 59%. These results underscore the critical role of current density in optimizing the effectiveness of electrocoagulation for organic matter removal in seawater. Despite the decrease in pH and the corresponding increase in H^+ concentration, the overall effect on electrical conductivity is minimal because the salinity and hardness of seawater are so high that their reduction cannot be fully offset by the decrease in pH. This suggests

Current density (mA/cm^2)	Final conductivity (mS/cm)	Final salinity (mg/L)	Final PH
2	52.5	34.8	7
4	52.3	34.8	6.8
8	52.1	34.7	6.7
12	52	34.5	6.6
16	51.9	34.4	6.3
20	51.9	34.4	6

Table 2. Final physicochemical parameters as a function of current density.

that the primary mechanisms for reducing salinity and conductivity involve the removal of dissolved salts through electrocoagulation, rather than the changes in pH[50]. These findings further emphasize the importance of optimizing the current density to enhance the removal efficiency of organic matter, as measured by both DOC and UV254 absorbance, during the electrocoagulation process. The results indicate that increasing the current density to 20 mA/cm^2 provided the highest removal rates for both DOC and UV254, with minimal changes observed beyond 80 min of treatment time. Additionally, the study demonstrates that the electrocoagulation process primarily affects the removal of dissolved salts, with only minor changes in electrical conductivity and salinity observed, even as the current density was increased. Overall, the study's findings highlight the critical role of current density in optimizing the effectiveness of electrocoagulation for organic matter removal in seawater, and provide insights into the underlying mechanisms responsible for changes in the physicochemical parameters of the treated water.

The electrocoagulation process was found to induce significant changes in pH, which were directly correlated with the increase in iron dosage (Fig. 8). These pH changes can be attributed to two primary mechanisms: electrochemical dissolution of iron electrodes and chemical shifts of H + and OH- ions[51]. The electrochemical dissolution of iron electrodes, triggered by the electric current, led to the release of Fe^{2+} and Fe^{3+} iron ions into the solution. Concurrently, chemical reactions occurred, resulting in the production or consumption of H^+ and OH^- ions. These changes in ion concentrations, in turn, caused a shift in the pH of the solution. The observed decrease in pH during the electrocoagulation process can be directly linked to the increase in iron dosage. This correlation suggests that the electrochemical dissolution of iron electrodes and the subsequent chemical shifts of H^+ and OH^- ions play a crucial role in pH changes during the electrocoagulation process. These findings provide valuable insights into the underlying mechanisms governing the electrocoagulation process and its impact on solution pH.

The observed decrease in pH during the electrocoagulation process can be attributed to several mechanisms. The precipitation of calcium carbonate and magnesium carbonate, resulting from the formation of carbonates, consumes hydroxide ions, leading to a decrease in pH. Additionally, at high current densities, the oxidation of chloride ions to chlorine gas is likely to occur, as described by the following reactions:

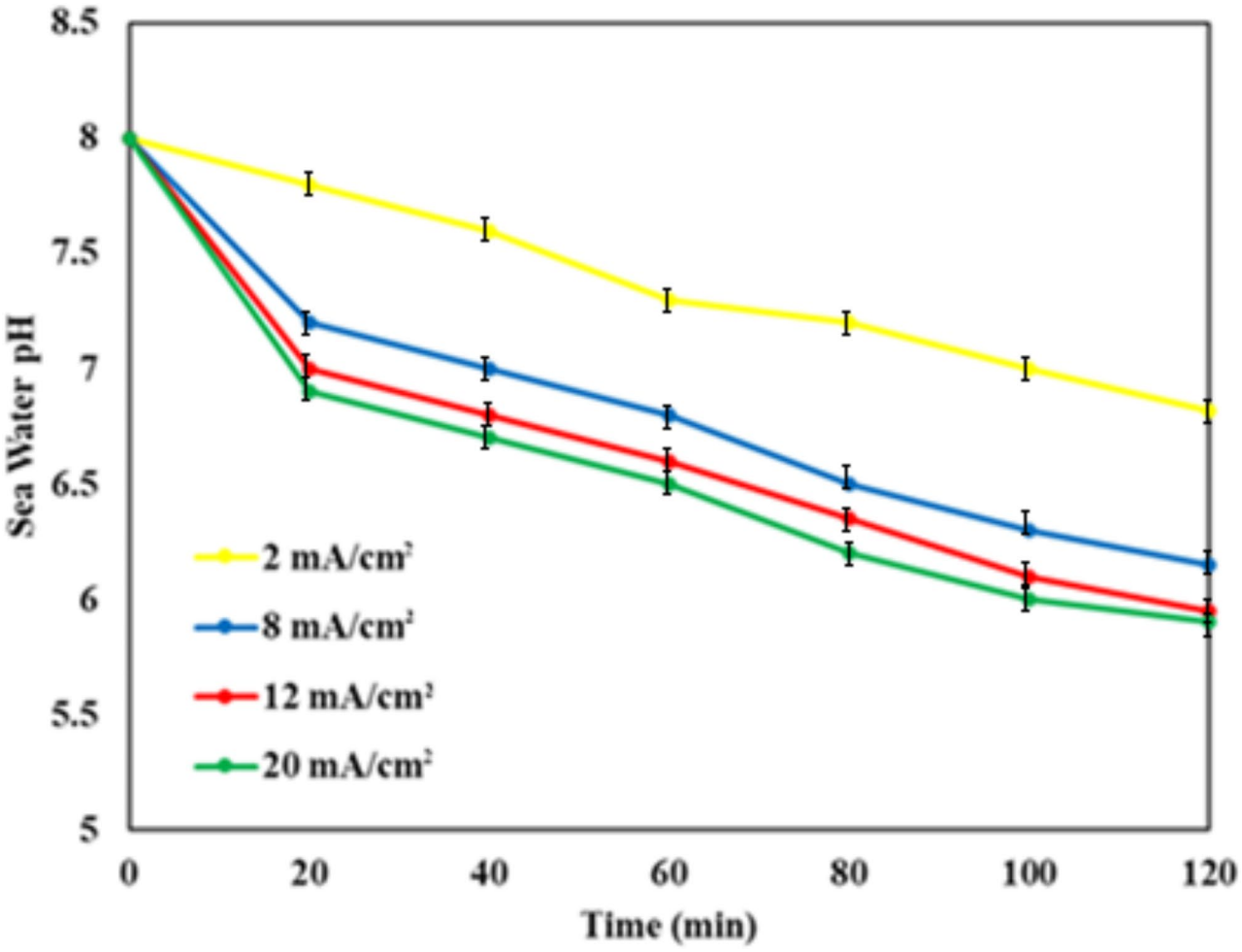

Fig. 8. Effect of current density on seawater pH with operating conditions including mixing speed = 90 rpm, electrode distance = 4 cm.

$$2Cl^{-}\,(aq) \rightarrow Cl_2\,(g) + 2e^{-} \quad (3)$$

$$2H_2O + 2e^{-} \rightarrow H_2\,(g) + 2OH^{-} \quad (4)$$

The resulting chlorine gas is then hydrolyzed to hypochlorous acid, which can dissociate to produce hydrogen ions, further contributing to the decrease in pH:

$$Cl_2\,(g) + H_2O \rightarrow HOCl\,(aq) + HCl \quad (5)$$

$$HOCl\,(aq) + H_2O \leftrightarrow H_3O^{+} + OCl\,(aq) \quad (6)$$

Furthermore, the chemical dissolution of electrodes releases iron cations, which consume electrochemically unproduced hydroxide ions, also contributing to pH reduction. Therefore, the decrease in pH can be attributed to the combined effects of calcium carbonate and magnesium carbonate precipitation, chloride ion oxidation, iron overload, and chemical dissolution of electrodes[52]. In contrast, the decrease in electrical conductivity appears to be primarily due to the removal of salinity by the electrocoagulation process, despite the decrease in pH. This decrease in conductivity is more pronounced at higher current densities. Notably, the initial pH has no significant effect on the final conductivity/salinity after electrocoagulation. These processes all lead to a decrease in the concentration of hydroxide ions, resulting in the observed reduction in pH. In contrast, the decrease in electrical conductivity appears to be primarily due to the removal of salinity by the electrocoagulation process, despite the decrease in pH. This decrease in conductivity is more pronounced at higher current densities. Notably, the initial pH has no significant effect on the final conductivity/salinity after electrocoagulation.

Effect of pH on electrocoagulation system

The initial pH of seawater plays a crucial role in the efficiency of electrocoagulation due to its impact on iron speciation, which results from the spontaneous hydrolysis of electrochemically produced metal cations. The effect of initial pH on the removal of dissolved organic carbon (DOC) and UV254 absorbance was investigated over a pH range from 4 to 10. As illustrated in the Fig. 9a and b, the removal efficiencies for DOC and UV254 increased with decreasing initial pH. The highest removal efficiencies were achieved at an initial seawater pH of 4. After 80 min of reaction time, the DOC removal efficiencies were 35%, 39%, 42%, and 47% for initial pH values of 10, 8, 6, and 4, respectively. Similarly, the UV254 removal efficiencies were 32%, 35%, 38%, and 47% for initial pH values of 10, 8, 6, and 4, respectively. These results indicate that lower initial pH levels enhance the electrocoagulation process's effectiveness in removing organic matter from seawater. The improved removal efficiency at lower pH can be attributed to more favorable conditions for the formation and activity of iron hydroxides, which play a key role in the coagulation and adsorption processes[53].

The natural organic matter (NOM) in seawater primarily comprises humic acids, including fulvic acid and humic acid, along with other humic-like compounds. The enhanced and faster removal of dissolved organic carbon (DOC) and UV254 absorbance at an initial pH of 4 during electrocoagulation can be attributed to the behavior of hydrolyzed iron species[54], the resulting electrocoagulation mechanisms, and the charge and solubility properties of humic-like compounds[55]. At different initial pH levels, the hydrolysis of iron cations (Fe^{2+} and Fe^{3+}) produced from anode electrolysis leads to the formation of positively charged iron hydroxides (such as $Fe(OH)_2$ and $Fe(OH)_3$) in acidic conditions. The active functional groups of humic acids include carboxyl and phenolic hydroxyl groups. At lower pH values, these groups retain their protonated forms (COOH and OH), while at higher pH values, they deprotonate to form carboxylate (COO^{-}) and phenolate (O^{-}) ions. At an initial pH of 4, the removal of DOC and UV254 is primarily driven by the charge neutralization of humic

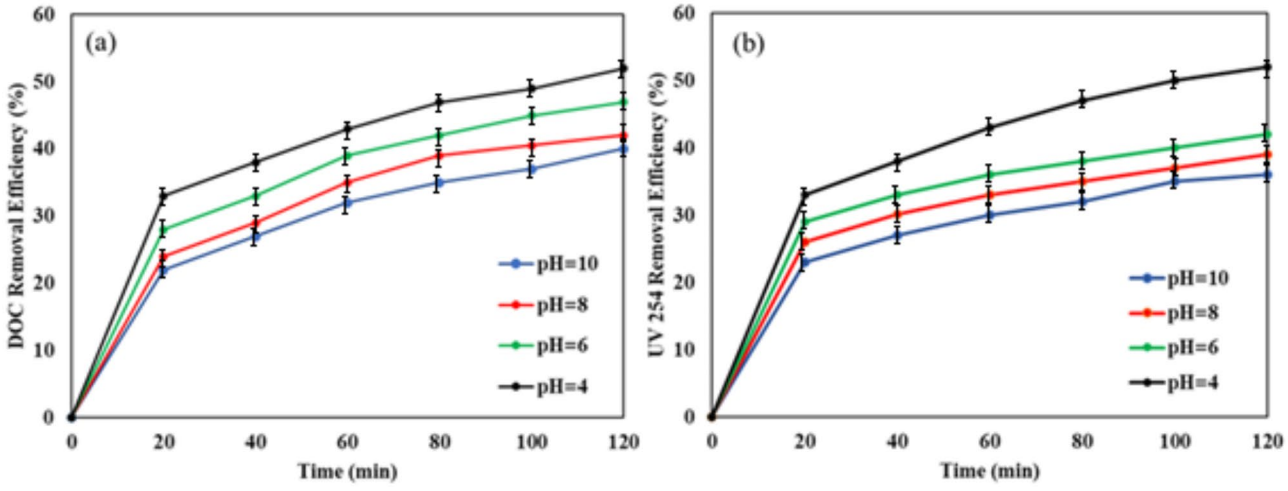

Fig. 9. The effect of sea water pH on the (**a**) DOC, (**b**) UV254 under the condition's current density = 12 mA cm^{-2}, mixing speed = 90 rpm, electrode distance = 4 cm.

acids and other organic components with similar functional groups. This leads to high removal efficiencies for DOC and UV254 due to the effective neutralization of the negatively charged organic matter by the positively charged iron hydroxides. In contrast, at higher (alkaline) pH levels, the deprotonation of humic compounds increases their negative charge and solubility. This higher negative charge reduces the efficacy of the positively charged iron hydroxides in neutralizing and removing the humic-like compounds[56]. Consequently, at alkaline pH levels, the dominant negatively charged iron hydroxides are less effective in intervening to remove humic substances. Therefore, DOC removal under these conditions primarily occurs through the adsorption of humic-like compounds onto insoluble iron hydroxides, resulting in lower removal efficiencies.

Effect of distance between electrodes in electrocoagulation system

The distance between the electrodes is a critical operational parameter that not only influences electrocoagulation performance but also affects the electric current input of the process, as the ohmic drop is directly proportional to the electrical resistance of seawater. To evaluate the effect of electrode distance (d) on seawater organic matter removal, several experiments were conducted. As illustrated in Fig. 10, smaller electrode spacings result in higher DOC removal efficiencies, primarily due to lower energy consumption. Previous research has attributed the high efficiency of electrocoagulation at short electrode distances to the enhanced buoyancy of iron-contaminant species facilitated by the electrolytic gas produced at the cathode. A shorter distance between electrodes creates an electric field with a high potential gradient and low resistance to ion movement. This configuration promotes the rapid formation of iron hydroxide species and accelerates the collision of deposited particles with pollutants and H_2 bubbles. In summary, the increased DOC removal efficiency at the smallest electrode distance is due to the enhanced mass transfer of species to the flocs, driven by the high turbulence observed near the electrodes. The DOC removal efficiencies for electrode distances of 2, 4, 8, and 10 cm were 46%, 39%, 34%, and 30%, respectively, within 80 min of reaction time.

The distance between the electrodes is a critical operational parameter in the electrocoagulation process, as it not only influences the performance but also affects the electric current input of the system. As illustrated in Fig. 10, the results show that smaller electrode spacings result in higher DOC removal efficiencies, primarily due to lower energy consumption. This observation can be explained by the following factors: the electrical

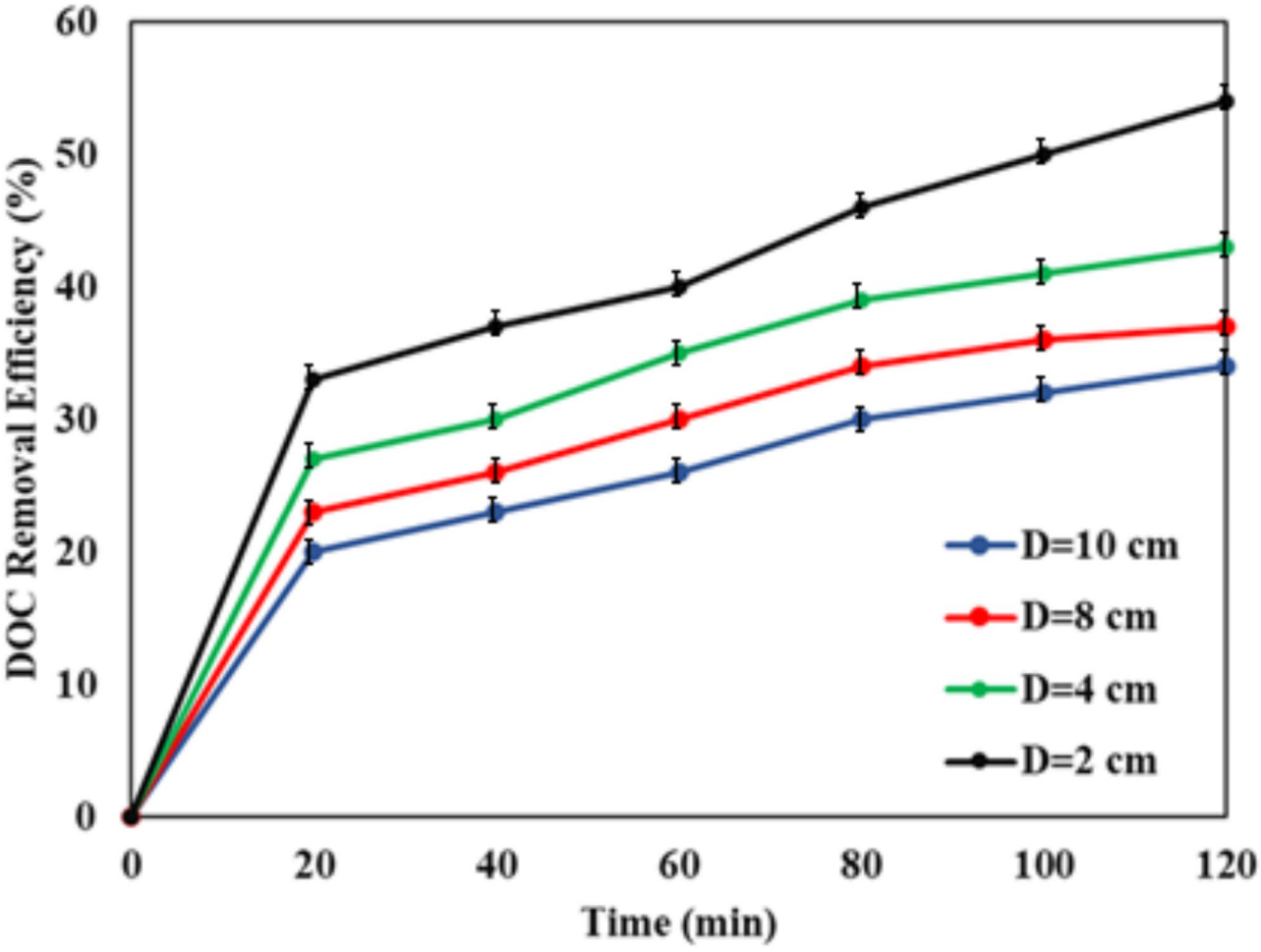

Fig. 10. Effect of electrode spacing on DOC removal rate with operating conditions: initial pH = 8, mixing speed = 90 rpm, current density = 12 mA cm-2.

resistance of the seawater is directly proportional to the distance between the electrodes (electrode spacing, d), and a smaller electrode spacing leads to a lower ohmic drop, which is the voltage drop across the seawater due to its electrical resistance[57]. The lower ohmic drop, in turn, results in a higher current input for the same applied voltage, enhancing the electrochemical reactions and the production of coagulating metal hydroxides. A shorter distance between the electrodes creates a stronger electric field with a higher potential gradient and lower resistance to ion movement[58], which promotes the rapid formation of iron hydroxide species and accelerates the collision of the deposited particles with pollutants and hydrogen bubbles[59].

Removing hardness in the electrocoagulation system

Water hardness is a prevalent issue caused by the presence of dissolved calcium (Ca^{2+}) and magnesium (Mg^{2+}) ions. The electrocoagulation process provides an effective mechanism for removing these hardness-causing ions through the in-situ production of coagulants via the electrolytic dissolution of sacrificial electrodes. Electrocoagulation with iron electrodes involves the anionic dissolution of the iron, which generates Fe^{2+} ions according to the following reaction:

$$\mathrm{Fe\,(s)} \rightarrow \mathrm{Fe^{2+}\,(aq)} + 2\mathrm{e^-} \tag{7}$$

These Fe^{2+} ions then undergo hydrolysis to form iron hydroxides, primarily $Fe(OH)_2$ and $Fe(OH)_3$, depending on the solution's pH. The formed iron hydroxides serve as coagulants, capable of adsorbing and precipitating calcium and magnesium ions, thereby reducing water hardness. The relevant reactions can be summarized as follows:

$$\mathrm{Fe^{2+}\,(aq)} + 2\mathrm{OH^-\,(aq)} \rightarrow \mathrm{Fe\,(OH)_2\,(s)} \tag{8}$$

$$4\mathrm{Fe\,(OH)_2\,(s)} + \mathrm{O_2\,(g)} + 2\mathrm{H_2O\,(l)} \rightarrow 4\mathrm{Fe\,(OH)_3\,(s)} \tag{9}$$

The $Fe(OH)_3$ flocs produced have a high specific surface area and strong adsorption capacity, which enhances the capture and removal of Ca^{2+} and Mg^{2+} ions from the water. This mechanism underlines the effectiveness of electrocoagulation in addressing water hardness by transforming dissolved ions into removable solid phases through coagulation and adsorption processes. The removal of total hardness from seawater by electrocoagulation was investigated to evaluate the efficacy of this pretreatment method in preventing scaling. Figure 11 illustrates the total hardness removal efficiency for different current densities over the treatment period. The results indicate that the total hardness removal efficiency from seawater is relatively low, ranging between 7.4% and 11.2%. Additionally, Fig. 11 shows that the removal efficiency does not significantly change with increasing current density and exhibits minimal improvement with prolonged treatment time beyond 20 min. This low removal efficiency can be attributed to the high total hardness of seawater, estimated to be between 2500 and 8000 mg/L. The high concentration of chloride anions in seawater mitigates the adverse effects of other anions such as CO_3^{2-} and SO_4^{2-}, preventing the deposition of compounds like $CaCO_3$, $CaSO_4$, $MgCO_3$, and $MgSO_4$. These compounds can form an insulating layer on the electrode surfaces, inhibiting effective electrocoagulation. However, the primary factor influencing the total hardness removal efficiency appears to be the saturation of the cathode surface by the precipitation of $CaCO_3$, $CaSO_4$, $MgCO_3$, and $MgSO_4$ after 20 min. This saturation, observed in Fig. 8, results in minimal improvement in removal efficiency over time. Figuratively, while electrocoagulation shows potential for reducing total hardness, its effectiveness is limited by the high initial hardness of seawater and the formation of insulating layers on the electrode surfaces[60].

The total hardness removal efficiency from seawater using electrocoagulation is relatively low, ranging between 7.4% and 11.2%, and does not significantly change with increasing current density or prolonged treatment time beyond 20 min. This low removal efficiency can be attributed to the high total hardness of seawater, estimated to be between 2500 and 8000 mg/L. Additionally, the high concentration of chloride anions in seawater mitigates the adverse effects of other anions, preventing the deposition of compounds like $CaCO_3$, $CaSO_4$, $MgCO_3$, and $MgSO_4$ on the electrode surfaces. The primary factor influencing the low total hardness removal efficiency is the saturation of the cathode surface by the precipitation of these hardness-causing compounds after 20 min of treatment. Briefly, the electrocoagulation process has limited effectiveness in removing total hardness from seawater due to the extremely high initial hardness, the mitigating effect of chloride ions, and the saturation of the electrode surfaces by the precipitation of hardness-causing compounds.

Conclusion

The electrocoagulation process has limited effectiveness in removing total hardness from seawater. The total hardness removal efficiency ranges between only 7.4% and 11.2%, and does not significantly improve with increasing current density or extended treatment times beyond 20 min. This low removal efficiency can be attributed to several interrelated factors. Firstly, the extremely high initial total hardness of seawater, estimated to be between 2500 and 8000 mg/L, poses a significant challenge for the electrocoagulation process to effectively remove the hardness-causing ions, calcium and magnesium. Additionally, the high concentration of chloride anions in seawater mitigates the adverse effects of other anions, such as carbonate and sulfate, preventing the deposition of hardness-causing compounds like calcium carbonate, calcium sulfate, magnesium carbonate, and magnesium sulfate on the electrode surfaces. The primary factor limiting the effectiveness of the electrocoagulation process is the saturation of the cathode surface by the precipitation of these hardness-causing compounds after just 20 min of treatment. This saturation inhibits the efficient operation of the electrocoagulation process and prevents any meaningful improvement in total hardness removal over extended treatment times. In summary, the combination of the extremely high initial hardness, the mitigating effect of chloride ions, and the

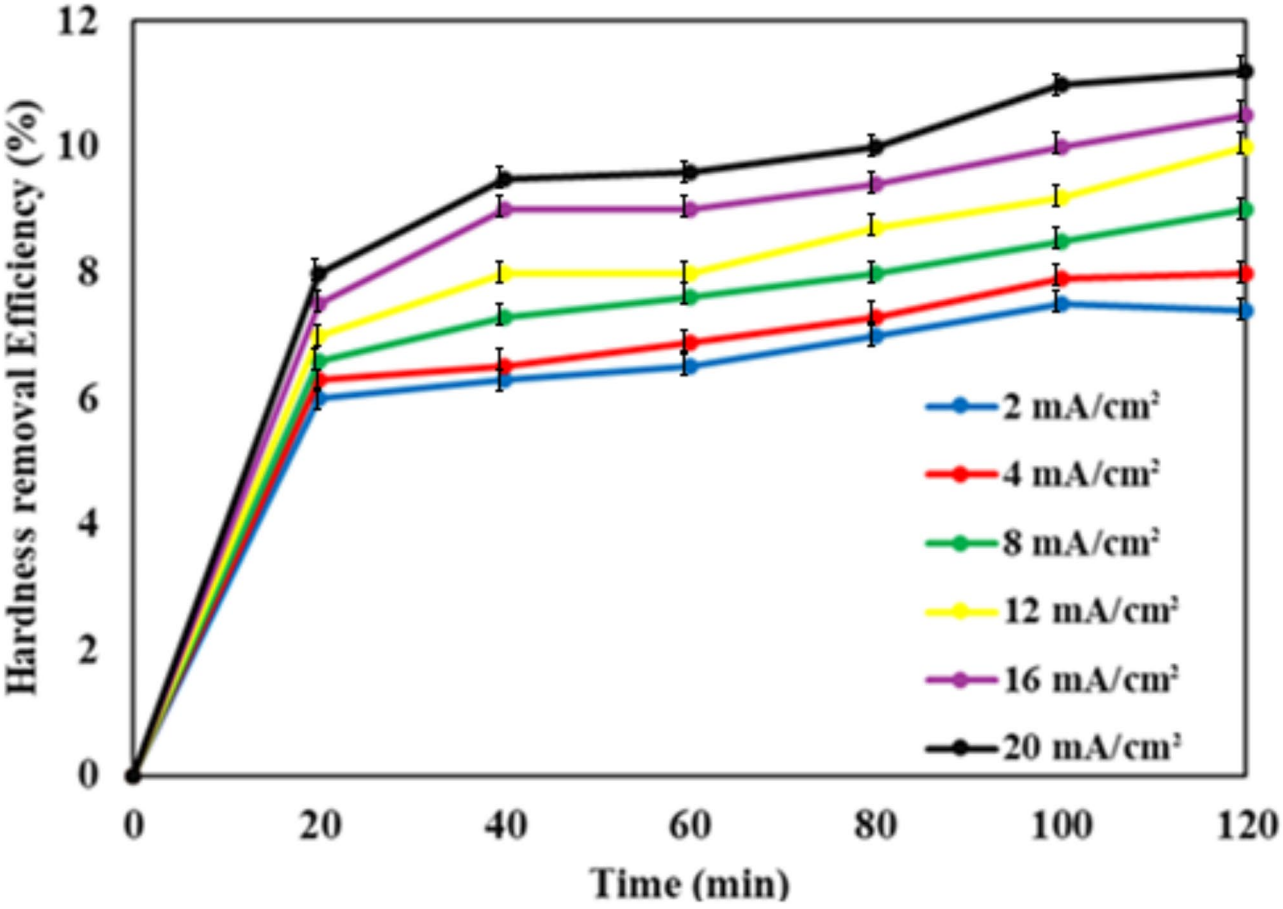

Fig. 11. Effect of current density on removal of total hardness from sea water with operating conditions including initial pH = 8, mixing speed = 90 rpm, electrode distance = 4 cm.

rapid saturation of the electrode surfaces by precipitated hardness-causing compounds collectively hinder the effectiveness of the electrocoagulation process in removing total hardness from seawater.

Data availability

All data generated or analyzed during this study are included in this article.

Received: 30 August 2024; Accepted: 5 March 2025
Published online: 10 March 2025

References

1. Ardhianto, R., Anggrainy, A. D., Samudro, G., Triyawan, A. & Bagastyo, A. Y. A study of continuous-flow electrocoagulation process to minimize chemicals dosing in the full-scale treatment of plastic plating industry wastewater. *J. Water Process. Eng.* **60**, 105217 (2024).
2. Chen, N. et al. Advanced Cr(VI) removal from wastewater using migrating electric field-assisted electrocoagulation combined with capacitive Deionization technology. *J. Water Process. Eng.* **63**, 105445 (2024).
3. Gabisa, E. W. & Ratanatamskul, C. Effects of operating conditions on removal of microplastics (PET, PP, PS) from wastewater by electrocoagulation systems and kinetics of chromium removal in the presence of microplastics. *J. Water Process. Eng.* **61**, 105313 (2024).
4. Liu, Z. et al. Faradaic efficiency and anodic electrochemical behavior of Fe electrocoagulation: The role of co-existing ions and ultrasonic assistance. *J. Water Process. Eng.* **57**, 104720 (2024).
5. Sadaf, S. et al. Electrocoagulation-based wastewater treatment process and significance of anode materials for the overall improvement of the process: A critical review. *J. Water Process. Eng.* **62**, 105409 (2024).
6. Tegladza, I. D., Xu, Q., Xu, K., Lv, G. & Lu, J. Electrocoagulation processes: A general review about role of electro-generated Flocs in pollutant removal. *Process Saf. Environ. Prot.* **146**, 169–189 (2021).
7. Vepsäläinen, M. & Sillanpää, M. Chapter 1 - Electrocoagulation in the treatment of industrial waters and wastewaters. in Advanced Water Treatment (ed Sillanpää, M.) 1–78 (Elsevier, doi:https://doi.org/10.1016/B978-0-12-819227-6.00001-2. (2020).
8. Issaka, E. From complex molecules to harmless byproducts: Electrocoagulation process for water contaminants degradation. *Desalin. Water Treat.* **319**, (2024).
9. Xu, J. et al. Enhancing the performance of the electrocoagulation-filtration system treating mariculture tailwaters by using alternating pulse current: effects of current density and current conversion period. *Water* **14**, (2022).
10. Kavitha, J., Rajalakshmi, M., Phani, A. R. & Padaki, M. Pretreatment processes for seawater reverse osmosis desalination systems—A review. *J. Water Process. Eng.* **32**, 100926 (2019).

11. Shirkoohi, M. G., Tyagi, R. D., Vanrolleghem, P. A. & Drogui, P. Artificial intelligence techniques in electrochemical processes for water and wastewater treatment: A review. *J. Environ. Health Sci. Eng.* **20**, 1089–1109 (2022).
12. Tang, J. et al. Electrocoagulation coupled with conductive ceramic membrane filtration for wastewater treatment: Toward membrane modification, characterization, and application. *Water Res.* **220**, 118612 (2022).
13. Sivasubramanian, P. et al. Capacitive Deionization and electrosorption techniques with different electrodes for wastewater treatment applications. *Desalination* **559**, 116652 (2023).
14. Keramati, M. & Ayati, B. Petroleum wastewater treatment using a combination of electrocoagulation and photocatalytic process with immobilized ZnO nanoparticles on concrete surface. *Process Saf. Environ. Prot.* **126**, 356–365 (2019).
15. Vignesh, R. V. & Sathiya, P. Sacrificial anode materials to protect marine grade steel structures: A review. *Corros. Rev.* **42**, 303–330 (2024).
16. Sajid, M. & Ihsanullah, I. Magnetic layered double hydroxide-based composites as sustainable adsorbent materials for water treatment applications: Progress, challenges, and outlook. *Sci. Total Environ.* **880**, 163299 (2023).
17. Muresan, L. M. Nanocomposite coatings for Anti-Corrosion properties of metallic substrates. *Materials* **16**, 5092 (2023).
18. Liu, F. et al. A systematic review of electrocoagulation technology applied for microplastics removal in aquatic environment. *Chem. Eng. J.* **456**, 141078 (2023).
19. Ali, Z. et al. Colorimetric sensing of heavy metals on metal doped metal oxide nanocomposites: A review. *Trends Environ. Anal. Chem.* **37**, e00187 (2023).
20. Ghamarpoor, R., Fallah, A. & Jamshidi, M. A. Review of synthesis methods, modifications, and mechanisms of ZnO/TiO2-Based photocatalysts for photodegradation of contaminants. *ACS Omega* **9**, 25457–25492 (2024).
21. Kan, M. et al. Photoelectrochemical seawater oxidation with metal oxide materials: Challenges and opportunities. *J. Energy Chem.* **97**, 767–782 (2024).
22. Hosseinkhani, O. et al. Graphene Oxide/ZnO nanocomposites for efficient removal of heavy metal and organic contaminants from water. *Arab. J. Chem.* **16**, 105176 (2023).
23. Mao, Y., Zhao, Y. & Cotterill, S. Examining current and future applications of electrocoagulation in wastewater treatment. *Water* **15**, 1455 (2023).
24. Naveas, N. et al. Antibacterial films of silver nanoparticles embedded into carboxymethylcellulose/chitosan multilayers on nanoporous Silicon: A Layer-by-Layer assembly approach comparing dip and spin coating. *Int. J. Mol. Sci.* **24**, 10595 (2023).
25. Mohammad, F. et al. Influence of surface coating towards the controlled toxicity of ZnO nanoparticles in vitro. *Coatings* **13**, 172 (2023).
26. Bordbar-Khiabani, A., Yarmand, B. & Mozafari, M. Enhanced corrosion resistance and in-vitro biodegradation of plasma electrolytic oxidation coatings prepared on AZ91 Mg alloy using ZnO nanoparticles-incorporated electrolyte. *Surf. Coat. Technol.* **360**, 153–171 (2019).
27. Talha, M. et al. Improved corrosion protective performance of hybrid silane coatings reinforced with nano ZnO on 316 L stainless steel. *Colloid Interface Sci. Commun.* **42**, 100411 (2021).
28. Bashir, S. et al. In-vivo (Albino Mice) and in-vitro assimilation and toxicity of zinc oxide nanoparticles in food materials. *Int. J. Nanomed.* **17**, 4073–4085 (2022).
29. Worku, A. K. et al. Structural and thermal properties of pure and chromium doped zinc oxide nanoparticles. *SN Appl. Sci.* **3**, 699 (2021).
30. Germination and Growth Characteristics of Mungbean Seeds. (Vigna radiata L.) affected by Synthesized Zinc Oxide Nanoparticles - Inpressco. https://inpressco.com/germination-and-growth-characteristics-of-mungbean-seeds-vigna-radiata-l-affected-by-synthesized-zinc-oxide-nanoparticles/
31. Mohora, E. et al. Removal of natural organic matter and arsenic from water by electrocoagulation/flotation continuous flow reactor. *J. Hazard. Mater.* **235–236**, 257–264 (2012).
32. Mousazadeh, M. et al. A systematic diagnosis of state of the Art in the use of electrocoagulation as a sustainable technology for pollutant treatment: an updated review. *Sustain. Energy Technol. Assess.* **47**, 101353 (2021).
33. Shimizu, A., Tokumura, M., Nakajima, K. & Kawase, Y. Phenol removal using zero-valent iron powder in the presence of dissolved oxygen: Roles of decomposition by the Fenton reaction and adsorption/precipitation. *J. Hazard. Mater.* **201–202**, 60–67 (2012).
34. Azerrad, S. P., Isaacs, M. & Dosoretz, C. G. Integrated treatment of reverse osmosis Brines coupling electrocoagulation with advanced oxidation processes. *Chem. Eng. J.* **356**, 771–780 (2019).
35. Das, P. P., Sharma, M. & Purkait, M. K. Recent progress on electrocoagulation process for wastewater treatment: A review. *Sep. Purif. Technol.* **292**, 121058 (2022).
36. Dayarathne, H. N. P., Angove, M. J., Aryal, R., Abuel-Naga, H. & Mainali, B. Removal of natural organic matter from source water: review on coagulants, dual coagulation, alternative coagulants, and mechanisms. *J. Water Process. Eng.* **40**, 101820 (2021).
37. He, S. & Jiang, S. P. Electrode/electrolyte interface and interface reactions of solid oxide cells: recent development and advances. *Progress Nat. Science: Mater. Int.* **31**, 341–372 (2021).
38. Lakshmanan, D., Clifford, D. A. & Samanta, G. Ferrous and ferric ion generation during Iron electrocoagulation. *Environ. Sci. Technol.* **43**, 3853–3859 (2009).
39. Deka, B. J., Guo, J., Jeong, S., Kumar, M. & An, A. K. Emerging investigator series: Control of membrane fouling by dissolved algal organic matter using pre-oxidation with coagulation as seawater pretreatment. *Environ. Sci. : Water Res. Technol.* **6**, 935–944 (2020).
40. Xu, L. et al. Highly efficient phosphorus removal by a novel prolonged stirring pelleting coagulation for sludge water treatment. *J. Water Process. Eng.* **64**, 105678 (2024).
41. Guo, K. et al. Insights into the mechanism of coagulation pretreatment for membrane fouling control from the perspective of organic removal based on a sensitive SEC-DAD-FLD-OCD/OND method. *ACS EST. Eng.* **3**, 851–861 (2023).
42. Abdollahi, J., Alavi Moghaddam, M. R. & Habibzadeh, S. The role of the current waveform in mitigating passivation and enhancing electrocoagulation performance: A critical review. *Chemosphere* **312**, 137212 (2023).
43. Bashir, Y., Raj, R., Ghangrekar, M., Nema, M. K., Das, S. & A. & Critical assessment of advanced oxidation processes and bio-electrochemical integrated systems for removing emerging contaminants from wastewater. *RSC Sustain.* **1**, 1912–1931 (2023).
44. Roy, D., Guha, S., Mal, S. & Ghosh, D. Chapter 4 - Electrochemical reduction of heavy metals from industrial effluents. in *Advances in Environmental Electrochemistry* (eds. Jadhav, D. A., Behera, M., Sevda, S. & Shah, M. P.) 89–122Elsevier, (2024). https://doi.org/10.1016/B978-0-443-18820-6.00006-0
45. Zhou, S. et al. Surface-growing organophosphorus layer on layered double hydroxides enables boosted and durable electrochemical freshwater/seawater oxidation. *Appl. Catal. B.* **332**, 122749 (2023).
46. Usman, M., Glass, S., Mantel, T., Filiz, V. & Ernst, M. Electro-sorption and -desorption characteristics of electrically conductive polyacrylonitrile membranes to remove aqueous natural organic matter in dead-end ultrafiltration system. *J. Water Process. Eng.* **58**, 104733 (2024).
47. Akash, S., Sivaprakash, B., Rajamohan, N. & Selvankumar, T. Biotransformation as a tool for remediation of polycyclic aromatic hydrocarbons from polluted environment - review on toxicity and treatment technologies. *Environ. Pollut.* **318**, 120923 (2023).
48. Tabash, I., Elnakar, H. & Khan, M. F. Optimization of iron electrocoagulation parameters for enhanced turbidity and chemical oxygen demand removal from laundry Greywater. *Sci. Rep.* **14**, 16468 (2024).
49. Ahmed, M. H. et al. Co-treating flue gas desulfurized effluent and produced water enables novel waste management and recovery of critical minerals. *Desalination* **585**, 117782 (2024).

50. Chen, M. et al. Boron removal by electrocoagulation: removal mechanism, adsorption models and factors influencing removal. *Water Res.* **170**, 115362 (2020).
51. Bonnefont, A. Deciphering the effect of pH on electrocatalytic reactions with kinetic modeling. *Curr. Opin. Electrochem.* **39**, 101294 (2023).
52. Zaldivar-Díaz, J. M. et al. Synergistic electrocoagulation–precipitation process using magnesium electrodes for denim wastewater treatment: Bifunctional support electrolyte effect. *J. Water Process. Eng.* **51**, 103369 (2023).
53. Yang, Z. et al. Chelated heavy metals removal by in-situ formed Fe(II) and Fe(III) iron (oxy)hydroxides: Mechanism and performance. *J. Environ. Chem. Eng.* **11**, 110531 (2023).
54. Lin, R. et al. Synergizing Fenton oxidation and in-situ coagulation over a wide pH range for the simultaneous removal of multiple pollutants. *Chem. Eng. J.* **454**, 140340 (2023).
55. Daraei, H. et al. Enhanced electrocoagulation process for natural organic matter removal from surface drinking water sources: Coagulant dose control & organic matter characteristics. *Environ. Science: Water Res. Technol.* **9**, 62–73 (2023).
56. Wen, S. et al. Composition regulates dissolved organic matter adsorption onto iron (oxy)hydroxides and its competition with phosphate: Implications for organic carbon and phosphorus immobilization in lakes. *J. Environ. Sci.* **144**, 159–171 (2024).
57. Eghbali, A., Karafi, M. R. & Sadeghi, M. H. The effects of current density, cell potential, time, salinity, electrode diameter, and material on Microwave-Assisted saline water electrolysis: An experimental study. *Water Conserv. Sci. Eng.* **8**, 13 (2023).
58. Cao, Q. et al. Gradient design of imprinted anode for stable Zn-ion batteries. *Nat. Commun.* **14**, 641 (2023).
59. Huang, Q. et al. Hydrogen nanobubbles generated in situ from nanoscale zerovalent Iron with water to further enhance selenite sequestration. *Environ. Sci. Technol.* **58**, 4357–4367 (2024).
60. Wang, X. et al. Coupled electrochemical crystallization-electrocoagulation-flocculation process for efficient removal of hardness and silica from reverse osmosis concentrate. *Desalination* **580**, 117549 (2024).

Acknowledgements

The authors are grateful for the supports provided by University of Imam Khomeini Marine Sciences.

Author contributions

All authors have contributed equally in the preparation of the manuscript. All authors reviewed the manuscript.

Declarations

Competing interests

The authors declare no competing interests.

Additional information

Correspondence and requests for materials should be addressed to S.N. or B.G.

Reprints and permissions information is available at www.nature.com/reprints.

Publisher's note Springer Nature remains neutral with regard to jurisdictional claims in published maps and institutional affiliations.